^{18}F-XTRA PET for Enhanced Imaging of the Extrathalamic α4β2 Nicotinic Acetylcholine Receptor

Jennifer M. Coughlin[1,2*], Stephanie Slania[3*], Yong Du[2*], Hailey B. Rosenthal[2], Wojciech G. Lesniak[2], Il Minn[2], Gwenn S. Smith[1,2], Robert F. Dannals[2], Hiroto Kuwabara[2], Dean F. Wong[1,2,4,5], Yuchuan Wang[2], Andrew G. Horti[2], and Martin G. Pomper[1–3]

[1]Department of Psychiatry and Behavioral Sciences, Johns Hopkins Medical Institutions, Baltimore, Maryland; [2]Russell H. Morgan Department of Radiology and Radiological Science, Johns Hopkins Medical Institutions, Baltimore, Maryland; [3]Department of Biomedical Engineering, Johns Hopkins Medical Institutions, Baltimore, Maryland; [4]Department of Neuroscience, Johns Hopkins Medical Institutions, Baltimore, Maryland; and [5]Department of Neurology, Johns Hopkins Medical Institutions, Baltimore, Maryland

Reduced density of the α4β2 nicotinic acetylcholine receptor (α4β2-nAChR) in the cortex and hippocampus of the human brain has been reported in aging and patients with neurodegenerative disease. This study assessed the pharmacokinetic behavior of ^{18}F-(−)-JHU86428 (^{18}F-XTRA), a new radiotracer for in vivo PET imaging of the α4β2-nAChR, particularly in extrathalamic regions of interest in which the α4β2-nAChR is less densely expressed than in thalamus. ^{18}F-XTRA was also used to evaluate the α4β2-nAChR in the hippocampus in human aging. **Methods:** Seventeen healthy nonsmoker adults (11 men, 6 women; age, 30–82 y) underwent PET neuroimaging over 90 or 180 min in a high-resolution research tomograph after bolus injection of ^{18}F-XTRA. Methods to quantify binding of ^{18}F-XTRA to the α4β2-nAChR in the human brain were compared, and the relationship between age and binding in the hippocampus was tested. **Results:** ^{18}F-XTRA rapidly entered the brain, and time–activity curves peaked within 10 min after injection for extrathalamic regions and at approximately 70 min in the thalamus. The 2-tissue-compartment model (2TCM) predicted the regional time–activity curves better than the 1-tissue-compartment model, and total distribution volume (V_T) was well identified by the 2TCM in all ROIs. V_T values estimated using Logan analysis with metabolite-corrected arterial input were highly correlated with those from the 2TCM in all regions, and values from 90-min scan duration were on average within 5% of those values from 180 min of data. Parametric images of V_T were consistent with the known distribution of the α4β2-nAChR across the brain. Finally, an inverse correlation between V_T in the hippocampus and age was observed. **Conclusion:** Our results extend support for use of ^{18}F-XTRA with 90 min of emission scanning in quantitative human neuroimaging of the extrathalamic α4β2-nAChR, including in studies of aging.

Key Words: ^{18}F-XTRA; PET imaging; nicotinic acetylcholine receptor; healthy aging

J Nucl Med 2018; 59:1603–1608
DOI: 10.2967/jnumed.117.205492

Nicotinic acetylcholine receptors (nAChRs) are pentameric ligand–gated ion channels, of which the α4β2 and α7 are the most abundant subtypes in the human brain. The loss of activity of even a small quantity of neuronal nAChRs can have wide-ranging effects on neurotransmission across neural circuits (*1*). Altered density of the α4β2-nAChR is linked to several neurodegenerative disorders (*2–5*). Additionally, postmortem work using ^{3}H-epibatidine (*6*) and some in vivo human imaging, including that using 2-^{18}F-fluoro-A-85380 (2-^{18}F-FA) with PET (*5,7*), suggest diminished availability of the α4β2-nAChR in human aging. The binding of 2-^{18}F-FA in the hippocampus and thalamus inversely correlated with performance on a cognitive task of processing speed in a cohort of elderly healthy participants (*8*).

There is need for α4β2-nAChR–targeting radiotracers with faster pharmacokinetics and high specific uptake in brain tissue outside the thalamus (extrathalamic regions such as the cortex and striatum) (*9,10*), in which the α4β2-nAChR is less densely expressed (*11*). ^{18}F-(−)-JHU86428 (^{18}F-XTRA) (*12,13*) is among such recently developed radioligands (*13–15*) and has promising in vitro binding characteristics, including subnanomolar binding affinity (K_i = 0.06 nM) and improved lipophilicity (Log$D_{7.4}$ = 0.67) over that of 2-^{18}F-FA (*13*). ^{18}F-XTRA also showed stable, high binding estimates in extrathalamic regions of the baboon brain in vivo (*12*).

This study assessed use of ^{18}F-XTRA with PET imaging in the human brain, particularly in extrathalamic regions of interest (ROIs). Estimates of total distribution volume (V_T) generated using kinetic modeling methods with arterial input function and using alternative scan durations were compared. Finally, we investigated the correlation between age and V_T in the hippocampus, a region in which low availability of the α4β2-nAChR may be linked to subtle deficits in cognition even in otherwise healthy older individuals (*8*).

MATERIALS AND METHODS

Human Subjects

This prospective study was approved by a Johns Hopkins Institutional Review Board, and all subjects provided written informed consent. Seventeen healthy adult (≥18 y) participants were recruited through local advertising. Each subject completed a screening interview and laboratory testing (blood counts, metabolic panel, coagulation studies), electrocardiogram, and urine toxicology. Eligible participants had stable health with no clinical abnormality on the screening assessment and structural MRI. Exclusion criteria included nicotine use in the past

Received Nov. 19, 2017; revision accepted Feb. 3, 2018.
For correspondence or reprints contact: Martin G. Pomper, 601 N. Caroline St., JHOC 3223, Baltimore, MD 21287.
E-mail: mpomper@jhmi.edu
*Contributed equally to this work.
Published online Mar. 1, 2018.

year, past psychiatric or neurologic illness, history of substance abuse including marijuana (assessed by self-report and urine toxicology), medication known to affect acetylcholine signaling, current psychotropic medication use, contraindication to MRI, or contraindication to PET imaging with arterial line.

All older (≥50 y) participants were also assessed with neuropsychologic testing that included the Clinical Dementia Rating scale (*16*) to ensure a global Clinical Dementia Rating of 0, consistent with normal cognition. Since the apolipoprotein ε4 (APOE ε4) allele may play a role in aberrant cholinergic signaling (*17*) that may be linked to altered α4β2-nAChR availability (*18*), older participants were assessed for APOE ε4 carrier status using methods described previously (*19*).

Human Brain Imaging

Synthesis of ^{18}F-XTRA. ^{18}F-XTRA was synthesized as previously described (*12*). Radiochemical purity was greater than 99%, with high specific radioactivity (1,586 ± 937 GBq/μmol) at the time of injection. The mean administered mass and radioactivity of ^{18}F-XTRA were 0.08 ± 0.04 μg (range, 0.03–0.17 μg) and 335 ± 38.3 MBq (range, 235–387 MBq), respectively. There were no adverse or clinically detectable pharmacologic effects, and no significant changes in vital signs, laboratory results, or electrocardiograms were observed.

Brain PET Image Acquisition. All participants wore a thermoplastic facemask to minimize head movement and underwent both radial arterial line and antecubital venous catheter insertion. PET scans were acquired using a High-Resolution Research Tomograph (Siemens Healthcare) with 2.5-mm reconstructed image resolution (*20*). Each emission scan started at the time of bolus intravenous injection of ^{18}F-XTRA, with continuous list-mode data collection for 90 (n = 10) or 180 (n = 7) min. Imaging data were reconstructed using methods described in the supplemental materials (available at http://jnm.snmjournals.org).

Plasma Sampling. Measurement of the arterial plasma input function was conducted through collection of 35–50 blood samples (1 mL), obtained after injection using the previously published protocol (*19*). Samples from 120 to 180 min after injection were collected every 10 min. Plasma was immediately isolated from whole blood using centrifugation. Radioactivity was counted in a cross-calibrated γ-well-counter. The fraction of parent radioligand in plasma was determined by high-performance liquid chromatography (HPLC) with blood sampling as previously described (*19*), with additional blood sampling at 105, 120, 150, and 180 min after injection for 180-min scans.

The modified column-switching HPLC method (*21*) used a Waters reverse phase XBridge BEH C18 5 μM 4.6 × 150 mm analytic column, with an analytic mobile phase (45% acetonitrile and 55% aqueous solution of 0.1% ammonium hydroxide) at 2 mL/min. The HPLC system was standardized using nonradioactive XTRA and ^{18}F-XTRA before analysis of plasma samples, which were spiked with 10 μL of XTRA (1 mg/mL) for each run. Metabolite-corrected plasma time–activity curves were obtained by applying percentage parent ligand time profiles, generated by HPLC analysis, to the total plasma time–activity curves after linear interpolation in PMOD (version 3.7; PMOD Technologies Ltd.).

MRI Acquisition. T1-weighted brain MRI at 3 T was acquired for each participant using methods identical to those as previously described (*19*), to obtain a 0.8 × 0.8 × 0.8 mm 3-dimensional image with a magnetization-prepared rapid gradient-echo sequence.

PET Image Analysis and Volumes of Interest. PET image processing, including motion correction and kinetic analysis, was conducted using PMOD as previously described (*19*). PET time–activity curves were generated for 10 ROIs that were segmented from each MR image using the FreeSurfer image analysis suite (http://surfer.nmr.mgh.harvard.edu/). ROIs included the thalamus, striatum, hippocampus, corpus callosum, as well as cerebellar, temporal, occipital, cingulate, frontal, and parietal cortices. Total intracranial volume was also defined using FreeSurfer for generating regional volume ratio values (ROI volume normalized to total intracranial volume).

Derivation of Rate Constants and V_Ts. V_T (*22*) for each ROI was derived using the metabolite-corrected arterial input function and compartmental modeling (1-tissue-compartment model with 3 parameters [1TCM]; 2-tissue-compartment model with 5 parameters [2TCM]) or Logan graphical analysis (*23*). In compartmental modeling, nonlinear least-squares analysis was performed, with the Marquardt algorithm for parameter estimation (*24*). Logan-derived V_T values were determined using ordinary least squares after transformation of the PET data with t* = 45 min. The contribution of cerebral blood volume was set at 5% of brain volume. As in other recent PET imaging of this target (*12,25*), reference-tissue models were not applied because there is no clearly identified human brain region devoid of the α4β2-nAChR.

Statistics

Compartmental model fitting was assessed by visual inspection of the model fit to the time–activity curves and by relative goodness of fit using the Akaike information criterion (*26*). The standard errors of nonlinear least-square estimates of rate constants and V_T from modeling were computed from the covariance matrix in PMOD and expressed as the coefficient of variation (% COV) (*27*). Regional V_T estimates from variable scan durations were evaluated using the 180-min acquisition as the reference for comparison of V_T values from data shortening (shortened to 90 min). For each duration, denoted X, relative bias values were expressed as $|V_{TX} - V_{T\ 180\ min}|/V_{T\ 180\ min}$.

The relationship between V_T in the hippocampus and age was tested using Spearman rank-order correlation analysis because age was not normally distributed across the study population. Secondary analyses testing the relationship between age and V_T in the other 9 ROIs were also explored.

Statistical analyses were performed using SPSS Statistics (version 23.0; IBM Corp.). Data were checked for outliers (*28*), and descriptive statistics were obtained. Normality of the data was assessed using the Shapiro–Wilk test. Data are presented as mean ± SD, and significance was set to a P value less than 0.05 unless otherwise noted.

RESULTS

Human Subjects

Seventeen healthy nonsmokers (11 men, 6 women; age, 30–82 y; median age, 60 y; interquartile range, 37 y) underwent PET neuroimaging with ^{18}F-XTRA (Table 1). All older participants (n = 10) had a global Clinical Dementia Rating of 0, and none of the participants was an APOE ε4 carrier. ROI volumes and volume ratios from the study population are presented in Supplemental Table 1.

Plasma Analysis

Plasma activity peaked within 90 s after injection and decreased to less than 5% of the peak by 20 min (Fig. 1A). HPLC easily isolated ^{18}F-XTRA (retention time, 7.5 min) from its radiolabeled metabolites,

TABLE 1
Clinical and Demographic Characteristics of 17 Healthy Human Participants

Characteristic	Mean or number
Mean age ± SD (y)	56.7 ± 19.6
Sex (male/female)	11/6
Race (Caucasian/African American/Asian)	9/7/1
Mean body mass index ± SD	26.3 ± 3.2

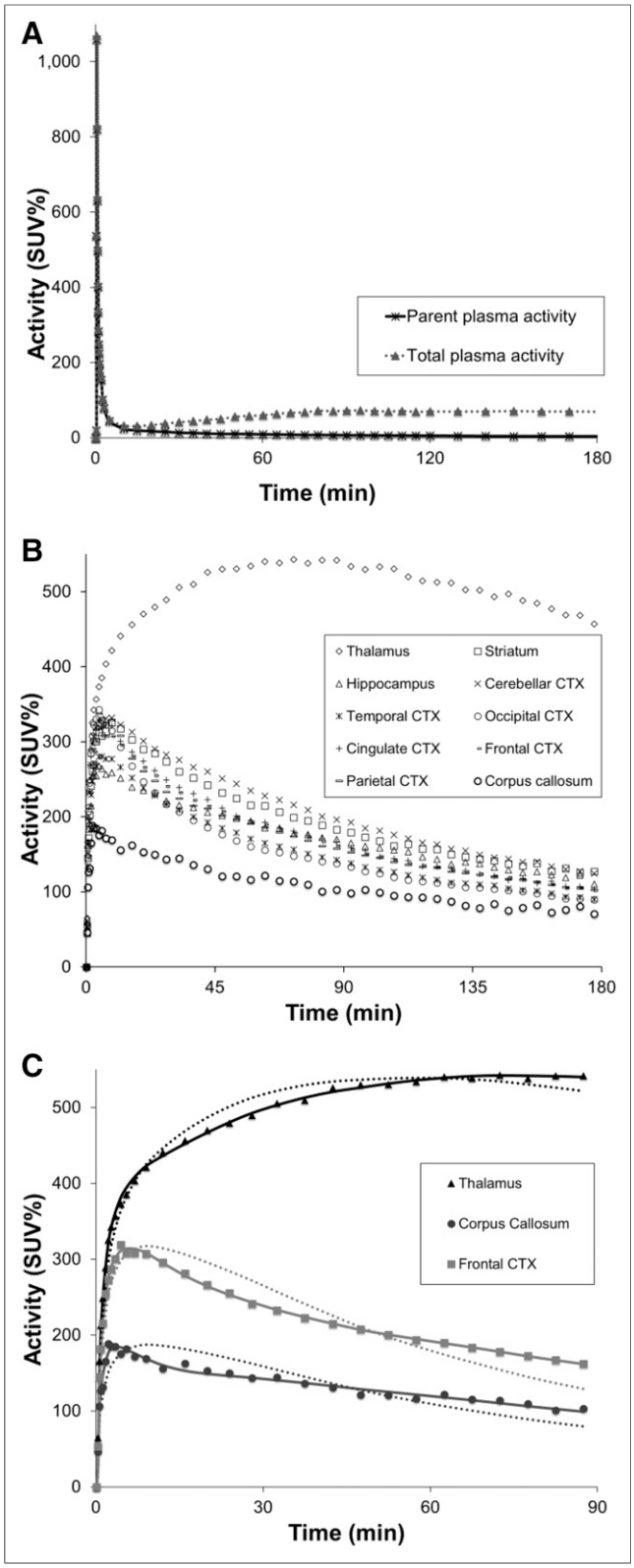

FIGURE 1. Time–activity curves from ^{18}F-XTRA imaging in a representative subject who underwent 180 min of continuous emission imaging. (A) Radioactivity curves in total plasma and in the portion of unmetabolized ^{18}F-XTRA parent are shown with activity shown as percentages of injected dose per mL plasma normalized to body weight in grams (SUV%). (B) Radioactivity curves spanning 180 min in 10 ROIs are shown. Time–activity curves are shown as percentages of injected dose per cm^3 tissue normalized to body weight in grams (SUV%). (C) The 2TCM showed better fit to observed tissue time–activity curves than the 1TCM in all ROIs. Observed activity (data in shapes) and model curves (solid curve, 2TCM; dotted curve, 1TCM) over 90 min from thalamus, frontal cortex, and corpus callosum are shown. CTX = cortex.

which were more polar and well resolved from the parent compound. ^{18}F-XTRA represented 21.8% ± 10.7% of total plasma activity by 90 min (Supplemental Fig. 1) and 15.2% ± 10.5% by 180 min.

Determination of V_T

^{18}F-XTRA readily entered the brain and, for extrathalamic ROIs, activity peaked within 10 min after injection and then declined over the remaining 90- or 180-min scan duration (Fig. 1B). Highest peak uptake occurred in the thalamus at approximately 70 min after injection except in 1 individual (a 76-y-old Caucasian man) whose thalamic activity peaked just before the end of the 90-min emission scan. Activity in the thalamus washed out gradually after the peak. The lowest uptake was observed in the corpus callosum.

Across the entire population, the kinetic behavior of ^{18}F-XTRA over the 90-min scan in each ROI yielded a visually better fit using the 2TCM compared with the 1TCM (Fig. 1C for representative data) except for within the thalamus of the aforementioned individual who had unusually late, 90-min peak thalamic activity that did not converge for either compartmental model. Those outlier data were excluded from further analyses, and when all other 90 min of continuous data were used, the Akaike information criterion favored the 2TCM in all 10 ROIs (Supplemental Table 2). The 2TCM identified V_T well (COV $<$ 5%) for all ROIs except for the thalamus, which had a COV of 5.4% (Table 2). K_1 was also identified well (COV $<$ 5%) using the 2TCM. The other rate constants from the 2TCM were identified with COV values of approximately 8%–22% for k_2 and 9%–24% for k_3/k_4 across all 10 ROIs. All V_T estimates (compartmental modeling, Logan) using 90-min emission data were highest in the thalamus and were more homogeneous across regions of the striatum, hippocampus, and cortical ROIs. V_T was lowest in the corpus callosum.

When 90-min data were used, values of regional V_T from Logan analysis correlated well with those of the 2TCM (Fig. 2). Regional V_T values generated using Logan analysis from the 90-min continuous scans were also within 5% of the V_T values obtained using 180 min of continuous data from the same 7 individuals (Fig. 3; Supplemental Table 3). Parametric images of V_T derived using Logan analysis from 90-min emission scans demonstrated binding of ^{18}F-XTRA throughout the brain (Fig. 4).

Correlation Between Age and V_T in Hippocampus

An inverse correlation between age and ^{18}F-XTRA V_T in hippocampus ($rho = -0.589$, $P = 0.014$) was found (Supplemental Fig. 2). Secondary analyses revealed no significant correlation between age and V_T in other ROIs after applying correction for multiple comparisons ($P < 0.005$ after Bonferroni adjustment for all 10 ROIs). There was also no correlation between body mass index and V_T in any of the ROIs. One-way ANOVA analysis revealed no effect of sex or race on V_T. There was no correlation between age and volume or volume ratio for any of the 10 ROIs.

DISCUSSION

PET imaging using newly developed radiotracers that have superior specificity for the α4β2-nAChR and faster brain kinetics

TABLE 2

Kinetic Parameters and Total Distribution Volume (V_T) Values Estimated with 2TCM, Along with V_T Values Estimated Using 1TCM and Logan Analysis for ^{18}F-XTRA PET Imaging in Humans (n = 17)

ROI	2TCM				1TCM, V_T (mL cm^{-3})	Logan, V_T (mL cm^{-3})
	K_1 (mL cm^{-3} min^{-1})	k_2 (min^{-1})	k_3/k_4 (unitless)	V_T (mL cm^{-3})		
Thalamus*	0.61 ± 0.10 (2.9 ± 1.6)	0.15 ± 0.11 (22.2 ± 12.0)	13.0 ± 8.1 (21.8 ± 11.2)	66.6 ± 17.4 (5.4 ± 9.7)	57.7 ± 13.4 (3.5 ± 1.1)	64.1 ± 18.4 (2.6 ± 1.0)
Striatum	0.52 ± 0.09 (1.8 ± 1.0)	0.07 ± 0.02 (9.6 ± 5.9)	1.29 ± 0.50 (13.6 ± 7.9)	17.3 ± 3.4 (4.6 ± 4.0)	14.5 ± 1.9 (2.6 ± 0.5)	16.7 ± 2.9 (1.1 ± 0.6)
Hippocampus	0.48 ± 0.07 (2.5 ± 1.3)	0.12 ± 0.05 (11.8 ± 5.9)	2.92 ± 1.22 (12.1 ± 5.9)	15.6 ± 1.9 (3.6 ± 2.6)	12.9 ± 1.5 (3.8 ± 0.6)	15.6 ± 2.0 (1.8 ± 0.5)
Cerebellar cortex	0.52 ± 0.07 (1.6 ± 0.9)	0.08 ± 0.03 (10.4 ± 5.2)	1.80 ± 0.53 (13.3 ± 6.5)	17.6 ± 3.0 (2.3 ± 2.9)	15.8 ± 2.3 (2.4 ± 0.5)	17.7 ± 3.1 (0.6 ± 0.3)
Temporal cortex	0.49 ± 0.08 (1.8 ± 1.3)	0.10 ± 0.05 (10.1 ± 7.6)	1.66 ± 1.01 (12.6 ± 8.1)	13.7 ± 2.2 (2.4 ± 2.5)	12.2 ± 1.9 (2.6 ± 0.5)	13.6 ± 2.3 (0.7 ± 0.3)
Occipital cortex	0.56 ± 0.08 (1.7 ± 1.3)	0.11 ± 0.04 (7.7 ± 6.0)	1.60 ± 0.80 (9.4 ± 6.4)	13.4 ± 2.1 (2.5 ± 2.3)	11.5 ± 1.9 3.2 ± 0.6)	13.2 ± 2.3 (0.7 ± 0.3)
Cingulate cortex	0.59 ± 0.09 (2.5 ± 1.6)	0.13 ± 0.08 (12.5 ± 7.8)	2.35 ± 1.56 (13.9 ± 7.1)	15.7 ± 2.9 (2.4 ± 2.3)	14.0 ± 2.4 (3.0 ± 0.5)	15.8 ± 3.1 (0.7 ± 0.3)
Frontal cortex	0.56 ± 0.08 (2.1 ± 1.5)	0.12 ± 0.07 (10.5 ± 7.9)	2.30 ± 1.65 (12.0 ± 7.2)	15.8 ± 3.1 (2.5 ± 2.4)	13.8 ± 2.5 (2.9 ± 0.5)	15.6 ± 3.3 (0.8 ± 0.5)
Parietal cortex	0.57 ± 0.09 (1.8 ± 1.2)	0.11 ± 0.05 (9.1 ± 6.2)	1.94 ± 1.07 (10.9 ± 6.1)	15.1 ± 2.7 (2.5 ± 2.4)	13.1 ± 2.3 (3.1 ± 0.6)	15.0 ± 3.0 (0.7 ± 0.3)
Corpus callosum	0.30 ± 0.06 (4.1 ± 1.8)	0.12 ± 0.06 (21.0 ± 8.5)	3.15 ± 2.12 (23.5 ± 9.9)	10.1 ± 1.7 (4.7 ± 4.5)	8.8 ± 1.5 (3.4 ± 0.7)	9.8 ± 1.6 (3.5 ± 2.0)

*One individual had poor fit for data from thalamus using all models tested, and these outlier data from thalamus of this individual were excluded. Regional V_T values were generated using metabolite-corrected arterial input function and 90-min dynamic data.

Data are mean ± SD, with %COV for each estimated parameter in parentheses.

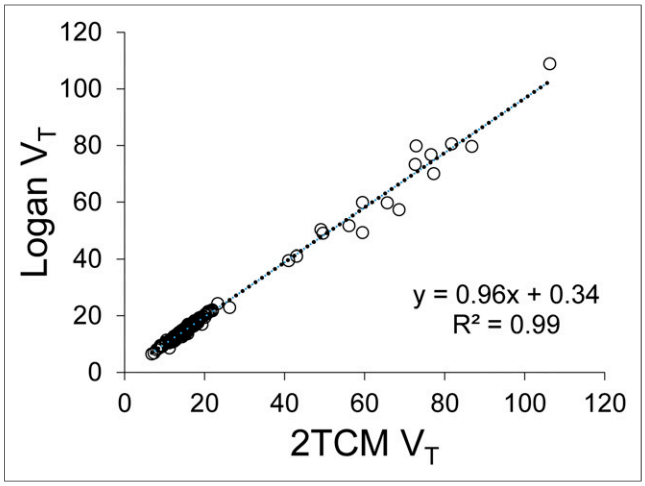

FIGURE 2. Comparison between ^{18}F-XTRA regional V_T values using 2TCM and Logan graphical analysis using 90-min data from 17 healthy individuals. After exclusion of outlier thalamic data from 1 individual, regional V_T values from 2TCM were highly correlated with those from the Logan method (Spearman *rho* = 0.986, P = 0.000). Results from secondary regression analysis are also shown. V_T is in units of mL cm^{-3}.

over previously used radioligands (*29*) may further our understanding of changes in cholinergic activity over the course of cognitive decline (*30*). Here we present the first human neuroimaging data using PET and ^{18}F-XTRA, a radiotracer with promising physical (*13*) and in vivo (*12*) characteristics.

^{18}F-XTRA readily accessed the brain in 17 healthy participants, all of whom underwent PET for 90 or 180 min. The highest uptake was in the thalamus, with relatively lower uptake in the striatum, hippocampus, and cortex and lowest uptake in the corpus callosum, consistent with direct assessment in postmortem tissue (*2*). After exclusion of thalamic data from 1 individual in whom thalamic activity peaked toward the end of the 90-min scan, V_T

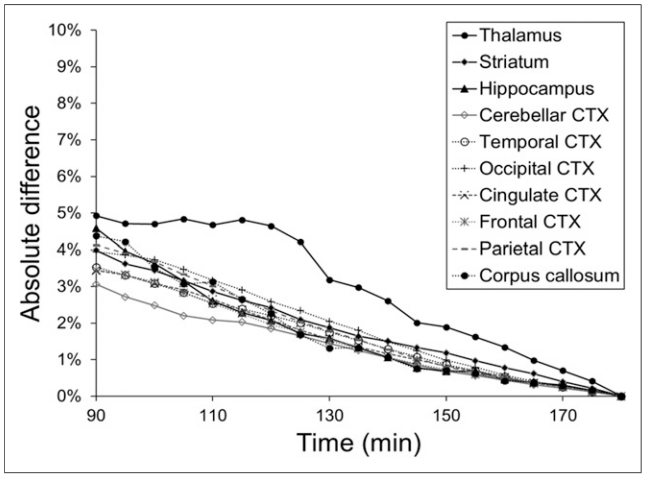

FIGURE 3. Assessment of relative stability in ^{18}F-XTRA regional V_T values from 180 min of data compared with values produced from truncated (by 5-min intervals down to 90 min) scan duration. Data from 7 healthy individuals who underwent 180-min emission scans were included. V_T estimates are in units of mL cm^{-3}. Percentage of absolute difference between V_T values from 180 min of data and V_T values from shortened scan duration are plotted for each of the 10 ROIs. CTX = cortex.

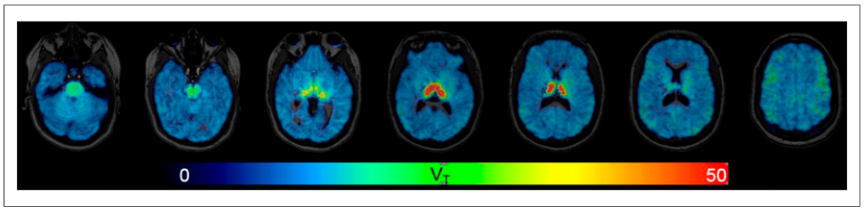

FIGURE 4. Parametric images of V_T of ^{18}F-XTRA, estimated using Logan graphical analysis with metabolite-corrected arterial input function and 90-min data from 1 representative healthy participant. Transaxial views of PET/MR images demonstrate high V_T values in thalamus and lower V_T values in other cortical and subcortical regions. There is no apparent region without binding of ^{18}F-XTRA.

values were well estimated using the 2TCM and 90-min acquisition, especially in extrathalamic regions. The 2TCM was favored over the 1TCM by goodness of fit and Akaike information criterion. The 2TCM V_T and K_1 values were well identified (COV $< 5\%$) in all extrathalamic regions and reasonably identified (COV $= 5.4\%$) in the thalamus. K_1 was also high ($K_1 > 0.48$ mL cm^{-3} min^{-1} in all cortical and subcortical ROIs; $K_1 = 0.30$ mL cm^{-3} min^{-1} in corpus callosum), consistent with high radiotracer delivery. Overall, the observed high uptake into the brain, fast pharmacokinetics, and ability to estimate V_T in extrathalamic regions with a 90-min scan supports further use of ^{18}F-XTRA in clinical research.

This initial evaluation of ^{18}F-XTRA in healthy humans revealed a negative correlation between age and V_T in the hippocampus. Since amyloid plaque may negatively influence expression of this receptor (*18*), all elderly (≥50-y-old) participants were evaluated for APOE ε4 carrier status. Those older individuals lacked even 1 APOE ε4 allele and were therefore at relatively low risk for having high amyloid burden. There was also no correlation between age and hippocampal volume or volume ratio among these participants. Together, our results suggest that ^{18}F-XTRA PET may be sufficiently sensitive to measure the hypothesized loss of α4β2-nAChR availability over aging in extrathalamic regions (*5–7*), particularly the hippocampus, in which reduced expression of the β2 subunit may account for the lower α4β2-nAChR binding in the elderly (*31*). This aging effect was not found using ^{18}F-nifene with PET, but this study population consisted of only 8 subjects (age, 21–69 y) (*32*).

^{18}F-XTRA V_T estimates were higher in most human extrathalamic brain regions than V_T values from bolus injection of other recently developed radiotracers with fast pharmacokinetics, such as (−)-^{18}F-flubatine (*25,33*) and ^{18}F-AZAN (*34*). Since V_T represents the sum of both specific binding and nondisplaceable uptake (*22*), we note the limitation that a displacement study, such as using nicotine, is needed to compare specific binding patterns between recently developed radiotracers. Limited blocking studies in baboons using ^{18}F-XTRA PET after subcutaneous administration of cytisine, a selective partial agonist at the α4β2-nAChR, support the specificity of this radiotracer for its target (*12*). Although ^{18}F-XTRA also has high affinity for the α6 nicotinic receptor subunit (*13*), central receptors containing the α6 subunit are relatively limited in distribution (retina, catecholaminergic nuclei) compared with the widespread, higher density of the α4β2-nAChR (*35*). We also note that thalamic data from 1 individual among the 17 participants did not peak until close to the end of the 90-min scan, rather than peaking at approximately 70 min. Since we saw a similar, late peak in thalamic data in 1 of 5 baboons (*12*), a conservative approach for studying the α4β2-nAChR in the human thalamus may use longer ^{18}F-XTRA scan duration (180 min) or use an alternative radiotracer that has not shown outlier thalamic pharmacokinetics, such as ^{18}F-AZAN (*34*).

CONCLUSION

^{18}F-XTRA is a promising new radiotracer for measuring the human cerebral α4β2-nAChR in vivo. Analysis by the 2TCM using ^{18}F-XTRA data from 90-min scan duration is sufficient to estimate V_T in extrathalamic ROIs, such as the cerebral cortex, hippocampus, and striatum. ^{18}F-XTRA PET is also a promising tool for further study of the effect of aging on the availability of the α4β2-nAChR, particularly in the hippocampus of the human brain in vivo.

DISCLOSURE

This work was supported by the Henry N. Wagner, Jr. Endowment (Martin G. Pomper), a Johns Hopkins Doris Duke Early Clinician Investigator Award (Jennifer M. Coughlin), the Alexander Wilson Schweizer Fellowship (Jennifer M. Coughlin), and the National Institutes of Health (R33AG037298 [Andrew G. Horti and Martin G. Pomper], AG038893 [Gwenn S. Smith], AG041633 [Gwenn S. Smith], Shared Instrument Grants S10RR023623 [Dean F. Wong], S10RR017219 [Dean F. Wong]). No other potential conflict of interest relevant to this article was reported.

ACKNOWLEDGMENTS

We thank the Johns Hopkins PET Center for expert provision of ^{18}F-XTRA (Daniel P. Holt, Robert C. Smoot, Jack C. Brown), with special thanks to Alimamy Kargbo for aid in the PET metabolite analyses.

REFERENCES

1. Dani JA. Overview of nicotinic receptors and their roles in the central nervous system. *Biol Psychiatry.* 2001;49:166–174.
2. Pimlott SL, Piggott M, Owens J, et al. Nicotinic acetylcholine receptor distribution in Alzheimer's disease, dementia with Lewy bodies, Parkinson's disease, and vascular dementia: in vitro binding study using 5-[(125)i]-a-85380. *Neuropsychopharmacology.* 2004;29:108–116.
3. Court J, Martin-Ruiz C, Piggott M, Spurden D, Griffiths M, Perry E. Nicotinic receptor abnormalities in Alzheimer's disease. *Biol Psychiatry.* 2001;49:175–184.
4. Sabri O, Kendziorra K, Wolf H, Gertz HJ, Brust P. Acetylcholine receptors in dementia and mild cognitive impairment. *Eur J Nucl Med Mol Imaging.* 2008; 35(suppl 1):S30–S45.
5. Meyer PM, Strecker K, Kendziorra K, et al. Reduced alpha4beta2*-nicotinic acetylcholine receptor binding and its relationship to mild cognitive and depressive symptoms in parkinson disease. *Arch Gen Psychiatry.* 2009;66:866–877.
6. Marutle A, Warpman U, Bogdanovic N, Nordberg A. Regional distribution of subtypes of nicotinic receptors in human brain and effect of aging studied by (+/−)-^{3}H-epibatidine. *Brain Res.* 1998;801:143–149.
7. Mitsis EM, Cosgrove KP, Staley JK, et al. Age-related decline in nicotinic receptor availability with ^{123}I-5-IA-85380 SPECT. *Neurobiol Aging.* 2009;30:1490–1497.
8. Sultzer DL, Melrose RJ, Riskin-Jones H, et al. Cholinergic receptor binding in Alzheimer disease and healthy aging: assessment in vivo with positron emission tomography imaging. *Am J Geriatr Psychiatry.* 2017;25:342–353.
9. Horti AG, Villemagne VL. The quest for Eldorado: development of radioligands for in vivo imaging of nicotinic acetylcholine receptors in human brain. *Curr Pharm Des.* 2006;12:3877–3900.
10. Horti AG, Kuwabara H, Holt DP, Dannals RF, Wong DF. Recent PET radioligands with optimal brain kinetics for imaging nicotinic acetylcholine receptors. *J Labelled Comp Radiopharm.* 2013;56:159–166.

11. Paterson D, Nordberg A. Neuronal nicotinic receptors in the human brain. *Prog Neurobiol.* 2000;61:75–111.
12. Kuwabara H, Gao Y, Stabin M, et al. Imaging alpha4beta2 nicotinic acetylcholine receptors (nAChRs) in baboons with ^{18}F-XTRA, a radioligand with improved specific binding in extra-thalamic regions. *Mol Imaging Biol.* 2017;19:280–288.
13. Gao Y, Kuwabara H, Spivak CE, et al. Discovery of (-)-7-methyl-2-exo-[3′-(6-^{18}F-fluoropyridin-2-yl)-5′-pyridinyl]-7-azabicyclo[2.2. 1]heptane, a radiolabeled antagonist for cerebral nicotinic acetylcholine receptor (alpha4beta2-nAChR) with optimal positron emission tomography imaging properties. *J Med Chem.* 2008;51:4751–4764.
14. Pichika R, Easwaramoorthy B, Collins D, et al. Nicotinic alpha4beta2 receptor imaging agents: part II. Synthesis and biological evaluation of 2-^{18}F-fluoro-3-[2-((S)-3-pyrrolinyl)methoxy]pyridine (^{18}F-nifene) in rodents and imaging by PET in nonhuman primate. *Nucl Med Biol.* 2006;33:295–304.
15. Smits R, Fischer S, Hiller A, et al. Synthesis and biological evaluation of both enantiomers of ^{18}F-flubatine, promising radiotracers with fast kinetics for the imaging of alpha4beta2-nicotinic acetylcholine receptors. *Bioorg Med Chem.* 2014;22:804–812.
16. Hughes CP, Berg L, Danziger WL, Coben LA, Martin RL. A new clinical scale for the staging of dementia. *Br J Psychiatry.* 1982;140:566–572.
17. Poirier J, Delisle MC, Quirion R, et al. Apolipoprotein E4 allele as a predictor of cholinergic deficits and treatment outcome in alzheimer disease. *Proc Natl Acad Sci USA.* 1995;92:12260–12264.
18. Wevers A, Burghaus L, Moser N, et al. Expression of nicotinic acetylcholine receptors in Alzheimer's disease: postmortem investigations and experimental approaches. *Behav Brain Res.* 2000;113:207–215.
19. Coughlin JM, Du Y, Rosenthal HB, et al. The distribution of the alpha7 nicotinic acetylcholine receptor in healthy aging: an in vivo positron emission tomography study with ^{18}F-ASEM. *Neuroimage.* 2018;165:118–124.
20. Sossi V, de Jong HWAM, Barker WC, et al. The second generation HRRT: a multi-centre scanner performance investigation. *IEEE Nucl Sci Symp Conf Rec.* 2005;4:2195–2199.
21. Hilton J, Yokoi F, Dannals RF, Ravert HT, Szabo Z, Wong DF. Column-switching HPLC for the analysis of plasma in PET imaging studies. *Nucl Med Biol.* 2000;27:627–630.
22. Innis RB, Cunningham VJ, Delforge J, et al. Consensus nomenclature for in vivo imaging of reversibly binding radioligands. *J Cereb Blood Flow Metab.* 2007;27:1533–1539.
23. Logan J, Fowler JS, Volkow ND, et al. Graphical analysis of reversible radioligand binding from time-activity measurements applied to [N-^{11}C-methyl]-(-)-cocaine PET studies in human subjects. *J Cereb Blood Flow Metab.* 1990;10:740–747.
24. Bevington PR, Robinson DK. *Data Reduction and Error Analysis for the Physical Sciences.* 3rd ed. New York, NY: McGraw-Hill; 2003.
25. Hillmer AT, Esterlis I, Gallezot JD, et al. Imaging of cerebral alpha4beta2* nicotinic acetylcholine receptors with (-)-^{18}F-flubatine PET: implementation of bolus plus constant infusion and sensitivity to acetylcholine in human brain. *Neuroimage.* 2016;141:71–80.
26. Akaike H. A new look at the statistical model identification. *IEEE Trans Automat Contr.* 1974;19:716–723.
27. Carson RE. Parameter estimation in positron emission tomography. In: Phelps ME, Mazziotta JC, Schelbert HR, eds. *Positron Emission Tomography and Autoradiography: Principles and Applications for the Brain and Heart.* New York, NY: Raven Press; 1986:347–390.
28. Hoaglin DC, Iglewicz B. Fine-tuning some resistant rules for outlier labeling. *J Am Stat Assoc.* 1987;82:1147–1149.
29. Horti AG, Wong DF. Clinical perspective and recent development of PET radioligands for imaging cerebral nicotinic acetylcholine receptors. *PET Clin.* 2009;4:89–100.
30. Volkow ND, Ding YS, Fowler JS, Gatley SJ. Imaging brain cholinergic activity with positron emission tomography: its role in the evaluation of cholinergic treatments in alzheimer's dementia. *Biol Psychiatry.* 2001;49:211–220.
31. Court JA, Martin-Ruiz C, Graham A, Perry E. Nicotinic receptors in human brain: topography and pathology. *J Chem Neuroanat.* 2000;20:281–298.
32. Mukherjee J, Lao PJ, Betthauser TJ, et al. Human brain imaging of nicotinic acetylcholine alpha4beta2* receptors using ^{18}F-nifene: selectivity, functional activity, toxicity, aging effects, gender effects, and extrathalamic pathways. *J Comp Neurol.* 2018;526:80–95.
33. Sabri O, Becker GA, Meyer PM, et al. First-in-human PET quantification study of cerebral alpha4beta2* nicotinic acetylcholine receptors using the novel specific radioligand (-)-^{18}F-flubatine. *Neuroimage.* 2015;118:199–208.
34. Wong DF, Kuwabara H, Kim J, et al. PET imaging of high-affinity alpha4beta2 nicotinic acetylcholine receptors in humans with ^{18}F-AZAN, a radioligand with optimal brain kinetics. *J Nucl Med.* 2013;54:1308–1314.
35. Quik M, Perez XA, Grady SR. Role of alpha6 nicotinic receptors in CNS dopaminergic function: relevance to addiction and neurological disorders. *Biochem Pharmacol.* 2011;82:873–882.